AIAA SciTech Forum
8–12 January 2018, Kissimmee, Florida
2018 AIAA/ASCE/AHS/ASC Structures, Structural Dynamics, and Materials Conference
10.2514/6.2018-0416

# High-Fidelity Trajectory Based MDO for the Conceptual Design of an Air-launched Spaceplane

Julien de Mûelenaere*, Juan J. Alonso †
*Stanford University, Stanford, CA, 94305, USA*



**This paper presents a Non-Linear-Programming-based All-At-Once Multidisciplinary Design Optimization (MDO) architecture for the conceptual design of an air-launched spaceplane. The optimization of the spaceplane geometry is coupled with the optimization of its trajectory, using SNOPT and GPOPS-II. High-Fidelity MDO in a conceptual design setting is investigated. A parametric geometry for the spaceplane is generated using GeoMACH. The aerodynamic coefficients are computed using the Reynolds-Averaged Navier-Stokes equations implemented in SU2. These are used to create a Kriging response surface. The weight of the spaceplane is estimated using TACS by performing a structural optimization. Most importantly, flight mechanics constraints, such as trim and stability, are imposed in order to size the planform of the wing as well as the control surfaces.**

## I. Introduction

Flexible, reliable and low cost access to space is one of the greatest challenges for today's aerospace sector. Prohibitive costs of current systems motivate the search for unconventional approaches and emphasize the importance of reusability. Notable examples of reusable space vehicles are the NASA Space Shuttle and the Boeing X-37B, which were intended to reduce the expenses of accessing Earth orbit for satellite delivery, science missions, or ferry to the International Space Station.

In a recent communication at the 2017 International Astronautical Congress in Adelaide, Australia, SpaceX Chief Executive Officer Elon Musk introduced the company's latest design of its Big Falcon Rocket. The upper stage, pictured in Fig. 1, now features a Delta Wing with a split flap aimed at controlling the pitch and roll moments.

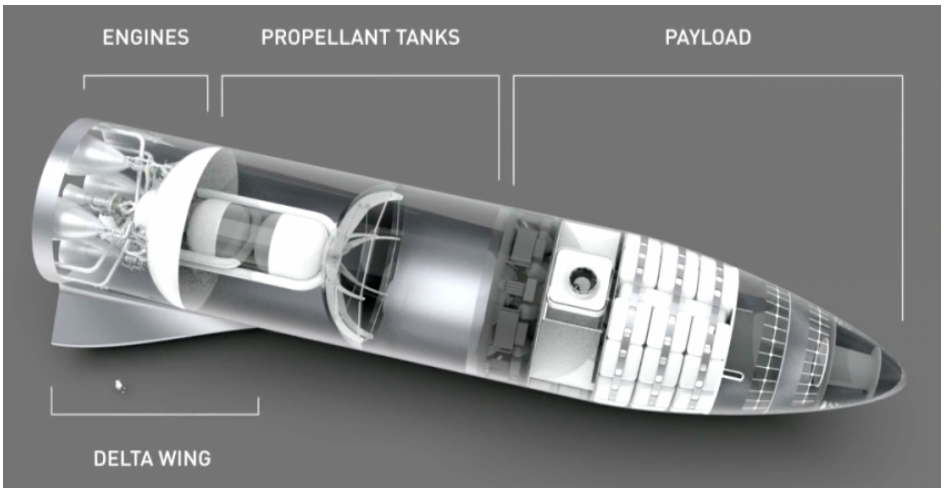


**Figure 1. Big Falcon Rocket's Upper Stage (SpaceX)**

*Graduate Student, Department of Aeronautics & Astronautics.
†Professor, Department of Aeronautics & Astronautics. AIAA Associate Fellow.

Even though the company tried to avoid adding the Delta Wing, it was necessary in order to expand the capabilities of the spaceship. The flaps allow to control the pitch angle of the spaceship as it enters the atmosphere, despite having a wide range of payloads in the nose and a wide range of atmospheric densities (Earth, Moon or Mars). This upper stage is essentially an air-launched spaceplane.

In this paper, a high-fidelity trajectory based Multidisciplinary Design Optimization (MDO) methodology for the conceptual design of an air-launched winged space vehicle, or spaceplane, is investigated. Depending on the mission, the spaceplane can either be orbital or suborbital, and can either be released from a carrier airplane or a first stage rocket booster.

Such a complicated system is intrinsically multidisciplinary. Because the design of a Reusable Launch Vehicle (RLV) involves multiple disciplines (structures, aerodynamics, trajectory, stability, etc.) that interact with one another, it requires multidisciplinary analysis and optimization. Good performance can only be achieved if trade-offs and synergies between different disciplines are carefully taken into account. A space vehicle also differs from more conventional industrial products where, for instance, it is possible to lump the limitations into a simple model like the Breguet equation.

By nature, the configuration of such vehicles is unconventional and model calibrations are not known. Optimization using high-fidelity physics-based models, such as Computational Fluid Dynamics (CFD) and Computational Structural Mechanics (CSM), is therefore essential. Trajectory-based MDO has been successfully applied to similar problems but with lower fidelity methods. Examples can be found in the works of Yokoyama et.al.,[1] Tsuchiya et.al.,[2,3] and Dufour et.al.[4]

This paper is organized as follows: Section II details how the baseline geometry is being generated. Section III provides an overview of the main disciplines covered in the MDO problem. In Section IV, a method to construct a surrogate model to approximate the computationally intensive disciplines is presented. Section V formulates the overall problem being solved while Section VI gives the MDO architecture being used. Section VII present the surrogate models specifically created for the problem of interest. Finally, Section VIII gives results.

## II. Geometry Generation

High-fidelity MDO in conceptual design requires a parametric representation of the aircraft which provides enough flexibility to generate a wide collection of configurations. Given that each discipline (aerodynamics, structures, stability, etc.) interacts with the aircraft geometry through either the Outer Mold Line (OML) or structural model, an easy to integrate conceptual-level geometry modeler, which facilitates communication among disciplines, is required.

Among other design tool suites, GeoMACH[5,6] (Geometry-centric MDAO of Aircraft Configurations with High fidelity) is capable of supporting high-fidelity MDO with hundreds of design variables. GeoMACH's OML modeler uses an efficient and lightweight B-spline engine presented in Hwang and Martins.[7] Its structural modeler models the aircraft as a thin-walled structure and has the ability to model detailed airframes including skins, spars, ribs, stringers, frames and longerons, while ensuring that the skin contains edges at location where an internal structural member intersects the skin. The aerodynamic and structural surface meshes are mapped linearly from the B-spline control points, and are automatically morphed in response to design variables change in the parametrically defined OML and structural models.

GeoMACH allows for the creation of arbitrary geometries from a handful of component classes including, among others: a Wing class, a Body class, and a Junction class. The Junction class is what enables GeoMACH's OML modeler to produce watertight geometries without computing intersections. Geometry engines that rely on intersections are not compatible with high-fidelity MDAO with many design variables as the intersections must be recomputed at each optimization iteration, and the surface mesh must be regenerated and topologically changed. With mesh regeneration, the only feasible approach is to use a gradient-free optimizer. When generating surrogate models, as is the case in Section IV, it is also recommended to use meshes which keep the same topology when varying the design variables. In this regard, GeoMACH is the candidate of choice for this study.

To be noted, in this study, the OML modeler was slightly modified to allow for a more flexible control surfaces design, which is essential to determine aircraft stability at the conceptual design level.

# III. Main Disciplines

Three main disciplines are being considered in the optimization of the spaceplane. The trajectory, the aerodynamics and the structure. This section describes those disciplines.

## III.A. Trajectory

The spaceplane is modelled dynamically as a point with variable mass flying around a rotating earth. A three-degrees-of-freedom (3DOF) trajectory analysis is implemented.

### *III.A.1. Acting Forces*

In order to compute the trajectory, we need to model the various forces acting on the spaceplane. Three types of forces are considered:

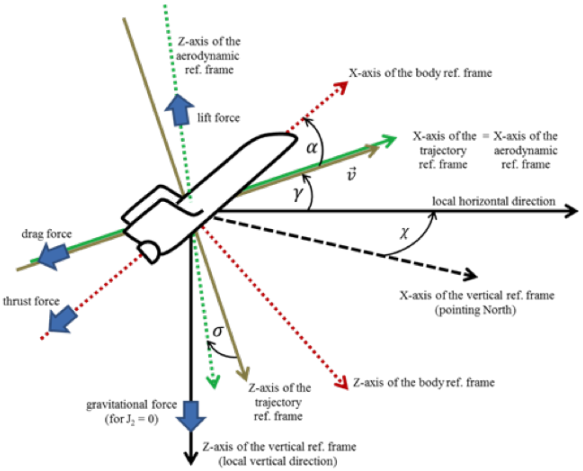


**Figure 2. Reference frames**

THRUST FORCE: The thrust force is modeled as:

$$T = T_0 - A_n p \tag{1}$$

where $T_0$ is the engine vacuum thrust, $A_n$ is the engine nozzle area, and $p$ is the atmospheric pressure. The thrust angle can be modified such as to achieve Thrust Vectoring Control (TVC).

GRAVITATIONAL FORCES: The gravitational forces are modeled as:

$$mg = [g_r, 0, g_\gamma]^T \tag{2}$$

where $m$ is the spacecraft's mass and $g_r, g_\gamma$ are the radial and meridional components of the Earth gravitational acceleration, respectively. The computation of the components of $g$ are aligned with the WGS84 standards and goes up to the 2nd zonal term ($J_2$).

AERODYNAMIC FORCES: The aerodynamic forces are modeled as:

$$L = 1/2\rho v^2 S C_l \tag{3}$$

$$D = 1/2\rho v^2 S C_d \tag{4}$$

where $\rho$ is the atmospheric density, $v$ is the airspeed velocity, $S$ is the reference surface, and $C_l, C_d$ are the coefficients of lift and drag, respectively.

Atmospheric properties, such as pressure, density and temperature are derived from the standard NRLMSISE-00 model. We assume a constant zero side-slip angle, therefore canceling the side-slip force and we take into account the plume effect, resulting from the gas exhaust of the main engine, by reducing the drag coefficient by 15% during propulsive phases.

### *III.A.2. Mass Properties*

The mass is assumed to vary linearly throughout the thrust phases of the flight. Mass variation is given by:

$$\dot{m} = -\frac{T_0}{I_{sp} g_0} \tag{5}$$

Where $I_{sp}$ is the engine specific impulse and $g_0$ is the Earth's gravitational acceleration at sea level.

### *III.A.3. Equations of motion*

Consider a frame of reference fixed with respect to the Earth and with its axis located at the Earth's center of mass. The Z-axis is co-linear with the Earth rotation axis and points towards the North, the X-axis points towards the zero-longitude meridian and the Y-axis completes the right-handed system. The equations of motion in this frame read:[8]

$$\begin{aligned}
\dot{r} &= v \sin(\gamma) \\
\dot{\lambda} &= \frac{v \sin(\chi) \cos(\gamma)}{r \cos(\phi)} \\
\dot{\phi} &= \frac{v \cos(\chi) \cos(\gamma)}{r} \\
\dot{v} &= \frac{1}{m} \left[ T \cos(\alpha) - D - m g_r \sin(\gamma) - m g_\gamma \cos(\gamma) \cos(\chi) \right] \\
&\quad + \omega^2 \cos(\phi) r \left[ \sin(\gamma) \cos(\phi) - \cos(\gamma) \sin(\phi) \cos(\chi) \right] \\
\dot{\gamma} &= \frac{1}{mv} \left[ \cos(\sigma)(L + T \sin(\alpha)) - m g_r \cos(\gamma) + m g_\gamma \sin(\gamma) \cos(\chi) \right] \\
&\quad + 2\omega \cos(\phi) \sin(\chi) + \frac{v \cos(\gamma)}{r} + \frac{r\omega^2}{v} \cos(\gamma) \left[ \cos(\phi) \cos(\gamma) + \sin(\gamma) \sin(\phi) \cos(\chi) \right] \\
\dot{\chi} &= \frac{1}{mv \cos(\gamma)} \left[ -\sin(\sigma)(L + T \sin(\alpha)) + m g_\gamma \sin(\chi) \right] \\
&\quad + 2 \frac{\omega}{\cos(\gamma)} \left[ \sin(\phi) \cos(\gamma) - \cos(\phi) \sin(\gamma) \cos(\chi) \right] \\
&\quad + \frac{v}{r} \cos^2(\gamma) \sin(\chi) \tan(\phi) + \frac{r\omega^2}{v \cos(\gamma)} \cos(\phi) \sin(\phi) \sin(\chi)
\end{aligned} \tag{6}$$

The state variables vector is given by the flight parameters [$r$, $\lambda$, $\phi$, $v$, $\gamma$, $\chi$, $m$], respectively the radial distance to the Earth's center, the geocentric longitude, the geocentric latitude, the co-rotational velocity, the flight-path angle (angle between velocity vector and local horizontal plane), the heading (angle between North direction and the projection of velocity on the local horizontal plane), and the vehicle mass. The longitude, latitude and heading are taken into account in order to add the effect of the Earth's angular velocity $\omega$ and Coriolis effect.

The control of the spacecrafts is achieved through the choice of angle-of-attack $\alpha$ and bank angle $\sigma$. These two angles define the orientation of the spacecraft in space.

### *III.A.4. Optimal Control Problem*

The control variables are optimized using a collocation method in order to minimize/maximize a functional of interest (mass injected into orbit, speed at main engine cut-off, etc.), while satisfying a set of physical and structural constraints.

In collocation methods, the state and control variables are discretized at a set of points chosen in the time interval. The continuous-time optimal control problem is then transformed into a finite-dimensional Non-Linear Programming problem (NLP) solved using optimizers such as SNOPT[9] which are able to deal with a large number of constraints.

GPOPS-II,[10] which implements a multiple-interval pseudo-spectral Legendre-Gauss-Radau (LGR) collocation method, was used in this study. LGR collocation method are said to lead to high accuracy in the

discretization and low computational costs.[11–14] The resulting sparse structure of the NLP allows for the use of a sparse non-linear programming techniques to further reduce the computational time.[14]

In addition, GPOPS-II employs hp-adaptive mesh refinement where the polynomial degree, number of mesh intervals, and width of each interval, can be varied. It allows for placement of collocation points in regions where additional information is needed.

### III.B. Aerodynamics

In this study, a high-fidelity formulation is chosen. A Reynolds-Averaged Navier-Stokes (RANS) formulation is being used with a two-equations Shear Stress Transport (SST) turbulence model. The differential equations are being solved using a Jameson-Schmidt-Turkel (JST) scheme for the spatial discretization and an Euler Implicit scheme for the time discretization.

The aerodynamic coefficients of the spaceplane are being computed using SU2,[15] a well-developed and validated open-source code suite. It integrates an unstructured finite-volume CFD code with parallel computation support. It is both a Direct and an Adjoint solver. The latter is particularly useful to perform sensitivity analysis when computing the gradients of a few functions with respect to many variables.

The surface meshes are generated using GeoMACH presented in Section II. The volume meshes are generated using GHS3D.[16] Subsequently, the density of the mesh is increased in regions of interest around the spaceplane using AMG,[17] a 3D anisotropic local re-mesher which uses a unique cavity-based operator for mesh adaptation. Finally a boundary layer is extruded using Bloom[18] with an initial spacing specified such that $y^+ = 1$ for the given freestream conditions.

### III.C. Structural Weight, Gross Weight and Center of Gravity Estimation

The weight of the spaceplane and the location of its center of gravity has a large impact on its performance and on the trajectory optimization procedure. Aerodynamic shape optimization alone is insufficient and a model of how the wing weight varies with respect to the design variables is required. This model is the result of an optimization process itself, where the weight of the structure is being minimized for each considered design point.

#### *III.C.1. Optimization problem*

The structural design problem considered is to minimize the structural weight $f(x)$ with respect to the structural thicknesses $x$ of each element, subject to stress, buckling, and/or displacement constraints $g_i(x)$ $(i = 1, ..., n_g)$ for a given wing planform and a set of aerodynamic and acceleration loads. The wing planform and loads are then varied to generate a weight model.

When conducted with high-fidelity methods, computing the gradients required for gradient-based optimization is computationally expensive. Adjoint sensitivity calculation of the constraints is preferred as it is much less expensive than direct sensitivity calculation.

In this study, we focus on the stress constraints. Constraints on admissible stresses are formulated to ensure that the yield strength $\sigma_{\text{yield}}$ is not exceeded during operating conditions. Von Mises stresses $\sigma_i^{\text{VM}}$ are used to indicate that the deformation is kept in acceptable ranges and the condition on finite element $i$ becomes

$$g_i(x) = \frac{\sigma_i^{\text{VM}}}{\sigma_{\text{yield}}} - 1 \leq 0 \tag{7}$$

#### *III.C.2. Constraints Aggregation*

When solving high-fidelity structural design problems, it is not feasible to formulate a separate condition at each finite element as the number of solutions required will render the overall problem intractable. A common approach[19] is to lump them into a reduced set of Kreisselmeier-Steinhauser (KS) functions that conservatively estimate the maximum of a set of stresses in a smooth and differentiable manner, and reduce the cost of adjoint sensitivity calculation. KS functions were first presented by G. Kreisselmeier and R. Steinhauser.[20]

Here, we use an alternate formulation[19,21] of the KS function which reduce numerical difficulties caused by numerical overflow

$$\mathrm{KS}\left(g_i(x)|_{i=1}^{n_g}\right) = g_{\max}(x) + \frac{1}{\rho}\ln\left[\sum_{i=1}^{n_g} e^{\rho(g_i(x)-g_{\max}(x))}\right] \tag{8}$$

where $\rho$ is a positive parameter controlling how close the function approximates the inequalities. When chosen too small, it results in a too conservative weight estimation (feasible designs according to the original set of constraints become infeasible). When $\rho$ is too large, it causes numerical difficulties.

### *III.C.3. Additional inertial loads*

In addition to the fuel, payload, and structure itself, other components must be considered in order to accurately estimate the overall gross weight of the spaceplane. These include the landing gear, the hydraulic, the avionics, the electrical systems, the equipments, the liquid oxygen and kerosene tanks, the engine, and the Thermal Protection System (TPS).

Empirical formulas from the Hypersonic Aerospace Sizing Analysis[22] (HASA) method have been used. The HASA method is a statistical weight approximation technique which has been shown to approximate correctly the gross takeoff weight for various types of hypersonic vehicles, including the NASA Space Shuttle. Due to improvement in structural materials and electronics over the years, some modifications were made to the original HASA method.

Most of the empirical formulas from HASA are iterative and require the unknown overall weight of the spaceplane as an input. Therefore, these are directly embedded in optimization problem described in Section III.C.1 in order to update the estimation at each iteration.

### *III.C.4. Non-inertial loads*

Aerodynamic loads (pressure and skin friction) on the CFD meshes are transfered to the structural meshes using the "mshint"[23] software. It features an interpolation operator on unstructured meshes that verifies the properties of mass conservation, P1-exactness (order 2) and maximum principle.[24]

Thrust loads from Eq. (1) are applied at different locations on the structure. The repartition between these points depends on the thrust-vectoring angle for which a simple truss problem is solved, where joints are assumed to act like hinges, permitting free rotation of the truss bars around the joints.

### *III.C.5. Software: TACS and SNOPT*

The Von Mises stresses and their sensitivities are obtained using the Toolkit for the Analysis of Composite Structures[25] (TACS). TACS is an integrated parallel finite-element analysis tool for gradient-based design optimization. Sensitivities are being calculated using an adjoint method. It solves large-scale high-fidelity structural optimization problems with thousands of design variables and hundreds of load cases. It is designed specifically for thin-walled metallic or composite structures, as is generally the case in high-performance aerospace applications. In this study, a thin-walled structure for the spaceplane was generated using GeoMACH presented in Section II. A third-order finite-element mesh is used to obtain accurate stress and strain distributions within the structure.

The optimization problem is solved using SNOPT[9] through the pyOptSparse interface. SNOPT is well-suited for large-scale constrained nonlinear optimization problems. The robustness of the SNOPT optimizer and its ability to solve ill-conditioned optimization problems allow to resort to large $\rho$ in the KS function definition, Eq. (8).

### *III.C.6. Center of gravity*

Once optimized, the position of the spaceplanes Center of Gravity (CoG) at dry condition is calculated using the weights and locations of each components. The CoG at any flight condition is then calculated in the trajectory analysis as the onboard fuel is consumed. Forward and Aft CoG limits are subsequently used to assess the longitudinal stability of the spaceplane.

# IV. Surrogate Model

The trajectory optimization requires the validation of thousands of constraints since the equation of motions are expressed as a set of equality constraints at every collocation point. These constraints and their Jacobian must be evaluated at every iteration.

In order to make the computational time practical while maintaining the solution accuracy, a series of surrogate models that give aerodynamic coefficients and mass estimate based on the geometric parameters and flight conditions are created before the optimization process. As it turns out, most of the computational cost is taken by the construction of the surrogate models, the computational cost of the optimization itself being much lower.

## IV.A. Kriging

A Kriging model, discussed in various publications,[26–32] is chosen for its ability to approximate multi-modal and highly nonlinear functions. It also has the advantage of providing both an estimated value and an associated uncertainty of the estimated value. This allows to increase the accuracy of the model by performing adaptive refinement, as will be discussed in Section IV.B.

Kriging is based on the assumption that the unknown function of interest $y(x)$, with $x$ an $n$-dimensional vector of design variables, can be modeled as a combination of a known trend function $\mu(x)$ and a departure from that function expressed as a Gaussian. The estimated value of $y(x)$ is expressed as

$$\hat{y}(x) = \hat{\mu}(x) + \bar{r}^T \bar{\bar{R}}^{-1}(\bar{y} - \bar{1}\hat{\mu}) \tag{9}$$

with $\hat{\mu}$ the estimated value of $\mu$, $\bar{y}$ a $N \times 1$ vector of sample values, and $\bar{r}$ and $\bar{\bar{R}}$ respectively the $N \times 1$ vector and $N \times N$ matrix of correlations between the current point $x$ and all $N$ sample points.

A variety of correlation functions can be used. The most common one in engineering applications is the Gaussian function

$$R(x^i, x^j) = \exp\left[-\sum_{k=1}^{n} \theta_k \left|x_k^i - x_k^j\right|^2\right] \tag{10}$$

proposed by Sacks.[33] It includes a $n \times 1$ correlation parameter vector $\bar{\theta}$ found by solving an optimization problem using maximum likelihood estimation,[34,35] and whose computational time increases exponentially as the number of sample points $N$ increases.

## IV.B. Construction method

As the number of sample points increases and the sample points become too close, the correlation matrix can become singular since the distance between any two sample points $i$ and $j$ in Eq. (10) decreases.

Kriging method therefore requires a sparse set of sample points, and an adequate construction method is needed. An initial set of points, 10 times the number of design variables $n$ in this study, is chosen using a space-filling design of experiments, in this case the Latin Hypercube Sampling method.[36] Once the initial Kriging model is constructed, a multi-modal optimization is carried out using a particle swarm optimizer (ALPSO[37] built into pyOpt[38]) to locate the point of maximum uncertainty. The response value is then evaluated at the new sample point in order the refine the Kriging model in an iterative process.

## IV.C. Surfpack

In this study, the Surfpack[32] library was chosen to build the Kriging models. Surfpack, which is developed at Sandia National Laboratories, is a general-purpose software library of multidimensional function approximation methods. It is primarily intended for use on sparse and irregularly-spaced data sets where classical function approximation methods are not applicable. In practice, Surfpack is generally targeted at applications with on the order of 10s to 100s of sample points, and 10s of dimensions,[32] which is the case in this study.

# V. Problem Formulation

This section presents the mathematical definition of the problem as well as the assumptions that were used to solve the optimization problem.

## V.A. Mission

As mentioned in the introduction, the air-launched spaceplane can either be orbital or suborbital, and can either be released from a carrier airplane or a first stage rocket booster. Applications for suborbital spaceplanes could either be space tourism, intercontinental long-haul flights, or release of an upper stage which is itself orbital.

In this paper, we propose to study a suborbital spaceplane mounted piggyback on a conventional airliner. The airliner lifts the mated configuration up to a scheduled separation altitude at which the spaceplane starts its ascent. It is propelled by its own rocket engine up to 100 kilometers. After all the fuel has burned, which is characterized by the Main Engine Cut-Off (MECO) point, the spaceplane enters a weightless ballistic flight phase.

## V.B. Vehicle Definition and Global Design Variables

Inspired by the NASA Space Shuttle and the Boeing X-37B, we decided to use a Double-delta Wing solution for the baseline geometry, as visible in Fig. 3. The geometry is generated using the GeoMACH design tool suite presented in Section II.

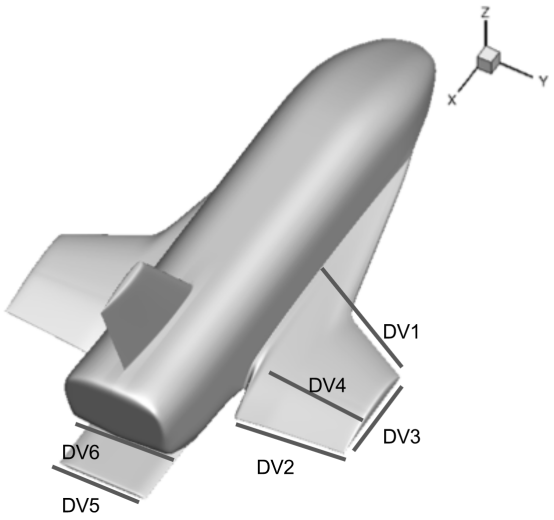


**Figure 3. Geometry definition and global design variables**

The global design variables $x$, shared across the disciplines, are defined such as to control the planform of the wing, and the hinge location and length of the control surfaces (elevons and body flap). As presented in Fig. 3, $DV1$ is the wing leading edge position, $DV2$ the elevon length, $DV3$ the wing span, $DV4$ the elevon hinge location, $DV5$ the body flap length and $DV6$ the body flap hinge location.

## V.C. Objective Function

In the case where the spaceplane is used for space tourism or intercontinental long-haul flights, maximizing the speed at main engine cut-off $v_{\text{MECO}}$ would allow for a longer weightlessness experience or a longer distance traveled, for a given amount of fuel.

In the case where the spaceplane is used to release an upper stage, the objective function should be to maximize the mass of the upper stage payload $m_{\text{PL}}$ brought to orbit for a given amount of fuel. The trajectory of the released upper stage solely depends on the flight conditions at the separation point, namely the flight-path angle $\gamma_{\text{SEP}}$, the speed $v_{\text{SEP}}$ and the altitude $h_{\text{SEP}}$. Therefore it is possible to optimize

independently the trajectory of the upper stage according to the separation conditions. As observed, when the injection window ($h_{\mathrm{SEP}}$, $\gamma_{\mathrm{SEP}}$) is fixed, as it is usually the case for a given mission, the injected mass is maximized when the velocity $v_{\mathrm{SEP}}$ is maximized. We can therefore decouple the upper stage trajectory optimization from our optimization problem.

Assuming separation and MECO happen at the same time, in either case, the objective function can be stated as

$$\max_x v_{\mathrm{MECO}}(x) \tag{11}$$

This state depends on the spaceplane global design variables $x$ form Section V.B and the optimal control solution for the spaceplane trajectory covered in Section III.A.

### V.D. Geometry related Constraints

The geometrical design variables are subjected to upper and lower bounds. Elevons and body flap deflection must range between -20 and 30 degrees.

### V.E. Mission related Constraints

The altitude $h_f$, longitude $\lambda_f$, latitude $\phi_f$ and heading of the runway $\chi_f$ at Edwards Air Force Base, California, are chosen as the final conditions for the mission. Landing velocity $v_f$ should not exceed the maximum velocity allowed by the tires, and be compatible with the length of the runway.

Initial conditions are as follows. The separation from the carrier airliner is chosen to occur in Nevada, at a longitude $\lambda_i$ and latitude $\phi_i$ such that the alignment with Edwards Air Force Base is compatible with the launch azimuth required for a sun-synchronous orbit, and the downrange compatible with an unpowered reentry. Release from the carrier occur at altitude $h_i = 10\,\mathrm{km}$, velocity $v_i = 210\,\mathrm{m/s}$ and flight-path angle $\gamma_i = -4\,\mathrm{deg}$.

MECO conditions are also imposed. The altitude $h_{\mathrm{MECO}}$ must be no less than 100 km and azimuth $\chi_{\mathrm{MECO}}$ compatible with a sun-synchronous orbit. The flight-path angle $\gamma_{\mathrm{MECO}}$ must also be constrained. When maximizing $v_{\mathrm{MECO}}$, the optimizer will have a tendency to increase the flight-path angle as it is easier to reach the targeted altitude with a higher flight-path angle. To be compatible with an orbit injection or long distance travel, $\gamma_{\mathrm{MECO}}$ must be no more than 20 deg.

### V.F. Structure related Constraints

In an effort to keep the structural loads to reasonable ranges, we are imposing constraints on the aero-heating, the load factor, and the dynamic pressure. A maximum heat flux of $80\,\mathrm{kW/m^2}$, a maximum load factor of 5, and a maximum dynamic pressure of 15 kPa are imposed.

### V.G. Aerodynamics and Flight Mechanics related Constraints

During the ascent, the vehicle is controlled solely by means of thrust vectoring and the control surfaces are considered to be always at their minimum drag position. However, during reentry, the spaceplane must be able to be aerodynamically trimmed and stable at angles of attack ensuring a high drag. This drag is necessary to maximize the energy dissipation before the more dense layers of the atmosphere are encountered, to limit the thermal and structural stresses, as expressed in Section V.F.

These trim and stability constraints will be the driving factors for the sizing of the control surfaces. In this paper, only longitudinal dynamics are considered. The roll angle and rate, and the sideslip angle and rate are always zero. As a result, only the longitudinal control surfaces (elevons and body flap) will be sized during the optimization. In some situations, shifting the spaceplane's center of gravity may also be necessary.

In this study, the following concepts, described in,[39–41] are being investigated.

#### *V.G.1. Aerodynamic Efficiency*

A minimum lift-to-drag ratio must be achieved in order to provide acceptable speeds and glide slope angles during the landing phase.

$$L/D = \frac{C_l}{C_d} \geq 5 \tag{12}$$

*V.G.2. Longitudinal Static Stability*

The static margin SM is defined as the distance between the neutral point (center of gravity location for which the pitch stiffness $C_{m_\alpha}$ goes to zero) and the center of gravity. When negative, the short period mode is a-periodically divergent. A divergence time of 0.5 seconds, corresponding to a static margin of -4%, is considered acceptable provided it will be stabilized by feedback control (Section V.G.3).

$$\text{SM} = -\frac{C_{m_\alpha}}{C_{z_\alpha}} \geq -4\% \tag{13}$$

*V.G.3. Longitudinal Stabilization*

The angle-of-attack feedback gain $K_\alpha$ describes the amount of artificial augmentation required to stabilize naturally unstable vehicles. It is desirable to maintain this gain value as low as possible to minimize surface activities and maintain the controller bandwidth to acceptable levels.

Expressing the Taylor series expansion of the pitch moment coefficient

$$\begin{aligned} C_m &= C_{m0} + C_{m_\alpha}\alpha + C_{m_{\delta_e}}\delta_e + ... \\ &= C_{m0} + C_{m_\alpha}\alpha + C_{m_{\delta_e}}K_\alpha\alpha + ... \\ &= C_{m0} + \left(C_{m_\alpha} + C_{m_{\delta_e}}K_\alpha\right)\alpha + ... \\ &= C_{m0} + C_{m_{\alpha_{\text{aug}}}}\alpha + ... \end{aligned} \tag{14}$$

we observe that the stability derivative $C_{m_\alpha}$ and control derivative $C_{m_{\delta_e}}$ can be lumped together to form the augmented stability derivative $C_{m_{\alpha_{\text{aug}}}}$ if the elevon deflection $\delta_e$ is controlled by the measured angle-of-attack $\alpha$ via the feedback gain $K_\alpha$. This gain is therefore expressed as

$$K_\alpha = \frac{C_{m_{\alpha_{\text{aug}}}} - C_{m_\alpha}}{C_{m_{\delta_e}}} \tag{15}$$

*Static Stabilization*

Given the definition of the Static Margin SM, the angle-of-attack feedback gain can also be expressed as

$$K_\alpha = \frac{\text{SM}_{\text{aug}} - \text{SM}}{C_{m_{\delta_e}}/C_{z_\alpha}} \leq 4\frac{\text{degrees}\,\delta_e}{\text{degrees}\,\alpha} \tag{16}$$

where $C_{m_{\delta_e}}/C_{z_\alpha}$ is a measure of the control surfaces effectiveness. For robustness considerations, we choose $\text{SM}_{\text{aug}} = 0.02$ and limit the feedback gain to be less than 4 $\frac{\text{degrees}\,\delta_e}{\text{degrees}\,\alpha}$.

*Dynamic Stabilization*

The augmented pitch stiffness $C_{m_{\alpha_{\text{aug}}}}$ in Eq. (15) is calculated from the desired frequency and damping. The undamped natural frequency $\omega_n$ and damping ratio $\zeta$ for the longitudinal short-period mode are[41]

$$\omega_n = \sqrt{-M_\alpha + \frac{Z_\alpha M_{\dot\theta}}{u_0}} \tag{17}$$

$$\zeta = -\frac{M_{\dot\theta} + M_{\dot\alpha} + \frac{Z_\alpha}{u_0}}{2\omega_n} \tag{18}$$

where the relationships between dimensional stability derivatives and dimensionless aerodynamic coefficients are given by $Z_\alpha = \frac{0.5\rho V^2 S}{m}C_{z_\alpha}$, $M_\alpha = \frac{0.5\rho V^2 Sl}{I_y}C_{m_\alpha}$, $M_{\dot\alpha} = \frac{0.5\rho V^2 Sl}{I_y}C_{m_{\dot\alpha}}$, $M_{\dot\theta} = \frac{0.5\rho V^2 Sl}{I_y}C_{m_{\dot\theta}}$, with $\alpha$

the angle-of-attack, $\theta$ the pitch angle, $\rho$ the density, $V$ the magnitude of the velocity, $S$ and $l$ the surface and length of reference, $m$ the mass, $I_y$ the moment of inertia, and $u_0$ such that $\alpha = \tan^{-1}\left(\frac{w}{u}\right) \approx \frac{w}{u_0}$.

Eq. (17) can be rearranged to read

$$C_{m_{\alpha_{\text{aug}}}} = \left(\frac{Z_\alpha M_{\dot{\theta}}}{u_0} - \omega_n^2\right) \frac{I_y}{0.5\rho V^2 S l} \tag{19}$$

To meet the flying qualities specified in MIL-STD-8785,[42] the value of the undamped natural frequency $\omega_n$ is chosen from the requirements of a Class IV (High-maneuverability), Category B (Nonterminal Flight Phases, normally accomplished using gradual maneuvers and without precision tracking), Level 1 (Flying qualities clearly adequate for the mission Flight Phase) aircraft.

This approach requires the computation of dynamic stability derivatives like $C_{m_{\dot{\alpha}}}$ and $C_{m_{\dot{\theta}}}$, and their gradients with respect to the geometric design variables. Techniques to numerically estimate those include, among others, modifying the CFD formulation to include the dynamic parameters, time-spectral methods, or harmonic balance solvers. Some of these approaches are covered in,[43,44] and are beyond the scope of this paper.

#### *V.G.4. Longitudinal Trim Capabilities*

It is desirable to rely as much as possible on the body flap. This leaves control margins for the elevons. Longitudinal trim shall be achieved with deflection of the body flap first and a maximum of 30% deflection of the elevons if the body flap is not enough.

$$\delta_e|_{C_m=0} \leq 30\% \tag{20}$$

## VI. MDO Architecture: NLP-based All-At-Once Problem

One approach is to take advantage of the fact that the Non-Linear Programming of the trajectory optimization already solves thousands of constraints as the equation of motions are expressed as a set of equality constraints at every collocation point. By adding the global design variables $x$ as control variables in the trajectory optimization, and by setting their derivatives with respect to time to zero in order to have a vehicle that remains to same throughout the mission, the optimizer is able to take into account all the design variables at once.

The NLP-based All-At-Once Problem is formulated as follows:

$$\max_x v_{\text{MECO}}(x)$$

Subject to:

- *Equality constraints*

  For the implicit integration of the equations of motion Eq. (6) presented in Section III.A.3.

- *Initial and final constraints for each phases*

  Mission related constraints presented in Section V.E

- *Connection conditions between phases*

- *Inequality path constraints*

  Structure related constraints presented in Section V.F: limitations on the dynamic pressure, load factor and aero-heating.

  Aerodynamics and Flight Mechanics related constraints presented in Section V.G: Eq. (12), (13), (16) and (20).

- *Static parameter constraints*

  Geometry related constraints presented in Section V.D

The optimizer, in this study SNOPT, for the trajectory optimization becomes the main driver of the MDO problem. The optimal solution gives the spaceplane's optimal geometrical variables as well as the optimal control solution for the spaceplane's ascent and reentry trajectories.

With this approach, all the nonlinear equations in the MDO problem are solved simultaneously without the need of inner iterations for each discipline, responsible for a slower rate of convergence.[45] The surrogate models approach makes it easy to embed the additional disciplines required by the newly added constraints. The surrogate models smoothness also contributes to the robust and fast convergence of the optimization.

# VII. Supporting Surrogate Models

## VII.A. Aerodynamics

As described in Section III.B, SU2 is used to generate a surrogate model for the lift, drag, axial force, normal force and pitch moment coefficients. In addition to the design variables $DV1-6$ presented in Section V.B, the surrogate models take the Mach number, Reynolds number, angle-of-attack, and elevons and body flap deflections as inputs.

To reduce the size of the domain, while ensuring that all flying conditions relevant to the problem will be covered, a change of variables for angle-of-attack and Reynolds number was performed, based on a reference trajectory.

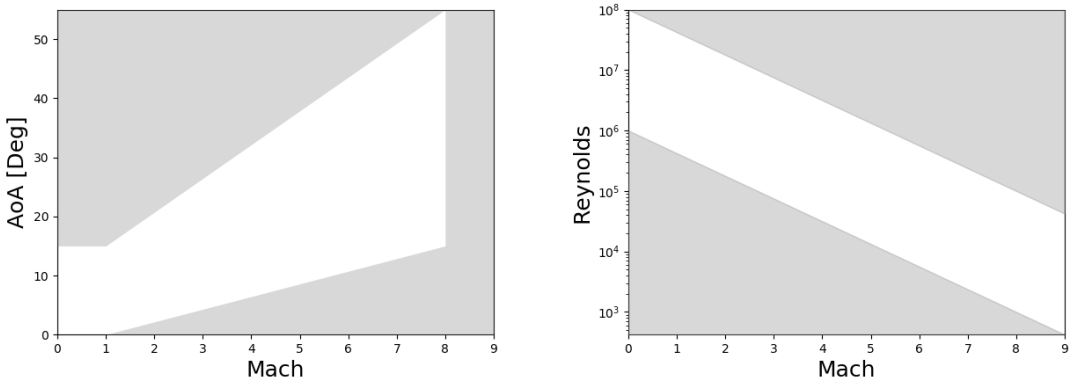


**Figure 4. Change of Variables**

Fig. 4 shows the change of variables. Flying conditions in the grayed area are never met in the reference trajectory. The change of variables for the angle-of-attack and the Reynolds number (which are Mach number dependent) are such that the upper bound of the white area is 1.0, and the lower bound is -1.0.

An example of pressure coefficient distribution for Mach 7.98, Reynolds 12.5E3, and angle-of-attack 31.14 degrees is shown in Fig. 5.

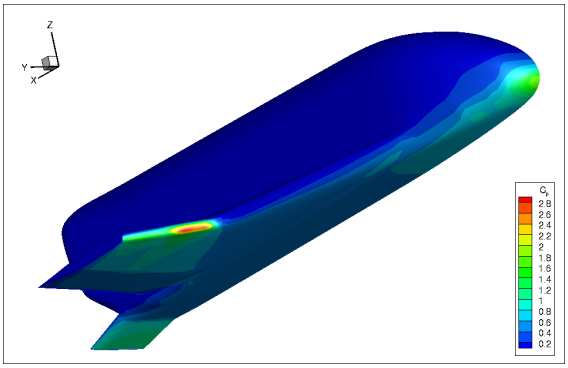

**Figure 5. Example of Cp distribution**

In order to reduce the number of cells in the boundary layer mesh and save computational time, the

vertical tail was not modeled in the CFD. This simplification is acceptable given that only longitudinal flight dynamics are considered in this study.

Surfpack, described in Section IV.C, was used to generate the 11-dimensional Kriging models with the construction method described in Section IV.B. Subsonic and supersonic regimes were considered separately. 510 design points were required to cover the supersonic regime, while 360 points were used for the subsonic regime. It is worth mentioning that to avoid any hysteresis effect, a fresh start was performed for each CFD computation.

As an example, Fig. 6 pictures lift, drag and pitch moment coefficients for the baseline geometry ($DV1-6=0.0$) with zero deflection control surfaces and zero variable changed Reynolds number.

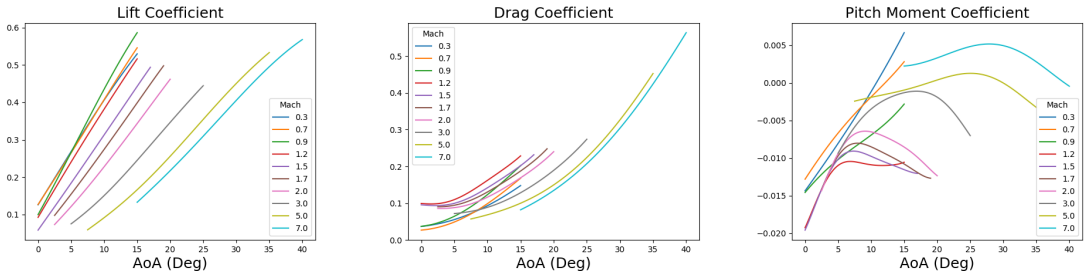


**Figure 6. Aerodynamic coefficients**

Surfpack also provides gradients with respect to the input variables, which will be useful to evaluate the stability derivatives $C_{m_\alpha}$ and $C_{z_\alpha}$, and the control derivative $C_{m_{\delta_e}}$.

## VII.B. Structure and Weight estimate

An overview of the geometry produced with GeoMACH, described in Section II, is given in Fig. 7. The structure is composed of skins, spars, ribs, stringers, frames and longerons, and features a wing box. Aluminum 2024-T3 with a density of 2780.0 kg/m$^3$, Young's modulus of 72.0 GPa, yield strength of 324.0 MPa, and Poisson ratio of 0.33 was chosen for the structure's material. A safety factor for the yield strength was applied in order to make sure that the ultimate tensile strength is never met in the operational envelope.

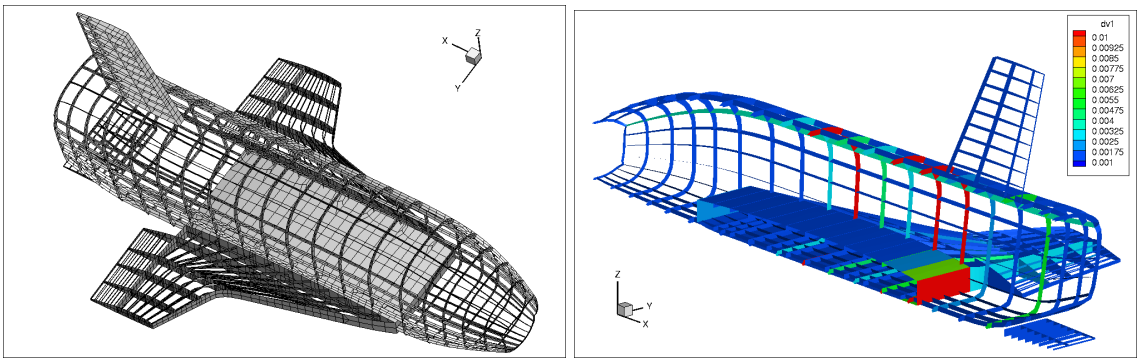


**Figure 7. Structure mesh (Skin elements not shown); Elements thicknesses**

The structural constraints are imposed at a series of design load cases to ensure the safety of the aerospace vehicle throughout the mission. Deduced from the reference trajectory in Fig. 8, three load cases are identified.

- Load Case 1: Ascent's Max dynamic pressure and normal acceleration

  Mach = 0.9, Reynolds = 6.8$e$6, AoA = 14.0 deg, $n_x = 0.81$, $n_y = 0.0$, $n_z = -1.80$, Fuel = 95%, Pdyn = 14.0 kPa, Thrust = 338.0 kN

- Load Case 2: Ascent's Max axial acceleration

  Mach = 8.0, Reynolds = 5$e$2, AoA = 2.5 deg, $n_x = 3.08$, $n_y = 0.0$, $n_z = 0.0$, Fuel = 0.5%, Pdyn = 0.0 kPa, Thrust = 400.0 kN

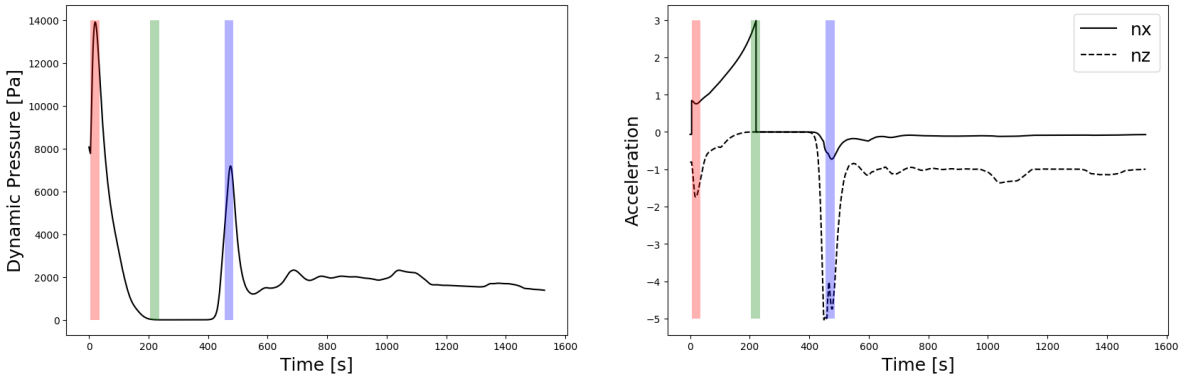


**Figure 8. Red: Load Case 1, Green: Load Case 2, Blue: Load Case 3**

- Load Case 3: Reentry's Max dynamic pressure and normal and axial acceleration

  Mach = 3.9, Reynolds = $9e5$, AoA = 22.5 deg, $n_x = -5.0$, $n_y = 0.0$, $n_z = -0.76$, Fuel = 0.0%, Pdyn = 7.3 kPa, Thrust = 0.0 kN

Each load case uses three KS functions: one for the skin elements, one for the members elements, and one for the junctions between the wings and the fuselage. Maximum Von Mises stress must be below the yield strength, which requires the three KS functions to be less than 1.

TACS was used to solve the structural optimization problem formulated in Section III.C. Feasibility and optimality tolerances for SNOPT were set to 10e-6. Structural design variables are the thicknesses of each component. A minimum thickness of 1.6 millimeters and a maximum thickness of 10 centimeters are defined for each design variable.

An example of convergence history is shown in Fig. 9. We observe that constraints from all 3 load cases are active at convergence, which emphasizes the importance of sizing the structure with respect to multiple load cases at the same time.

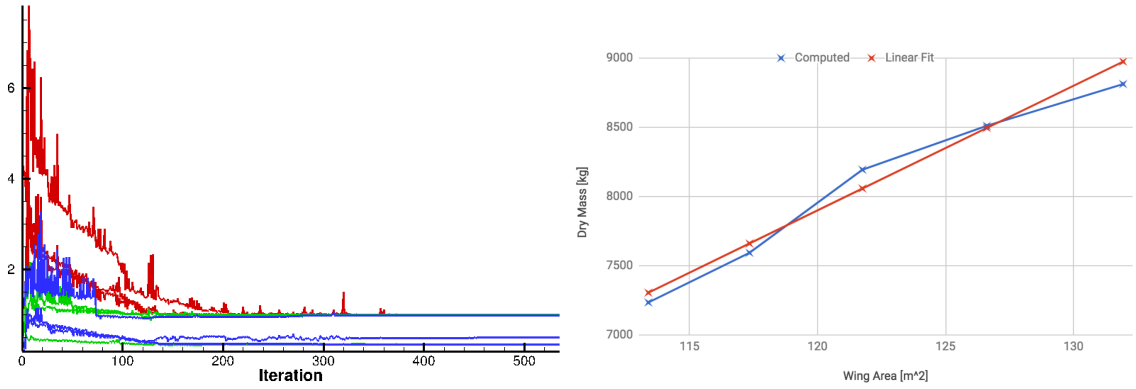


**Figure 9. KS Constraints (Red: Load Case 1, Green: Load Case 2, Blue: Load Case 3); Mass Model**

The load cases are themselves bounded by the max values imposed by the constraints of Section V.F. Even though the load cases will vary as the trajectory is iteratively modified during the optimization, we can assume, as a first step, that these variations will remain small. In this paper, a simplified surrogate model for the weight estimate is solely dependent on the wing area, as shown in Fig. 9. In future work, input variables to the surrogate model will include all geometric design variables independently, as well as varying load cases conditions.

## VIII. Results

An example of converged trajectory is given in Fig. 10. The red line represents the powered phase, and the blue line shows the unpowered gliding trajectory. A time history for the main quantities of interest is

shown in Fig. 11.

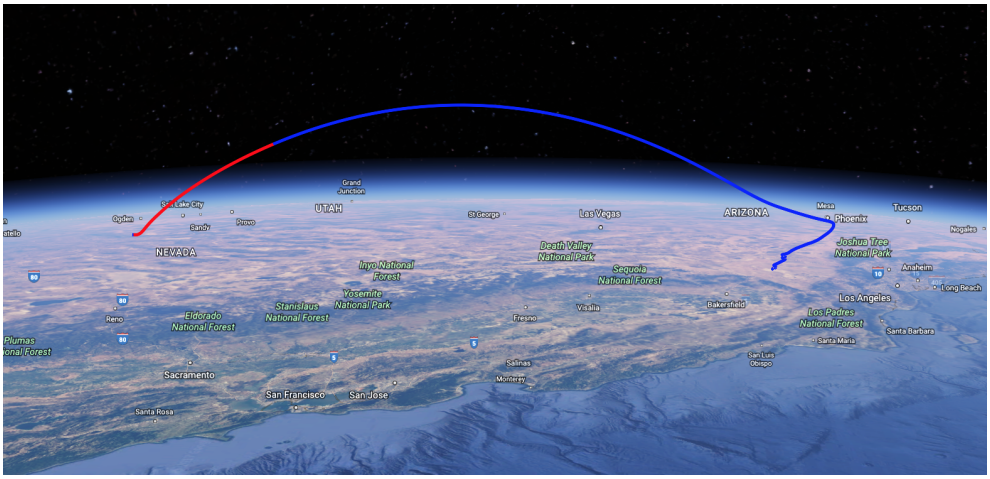


**Figure 10. 3D View of the trajectory (Red: powered, Blue: unpowered)**

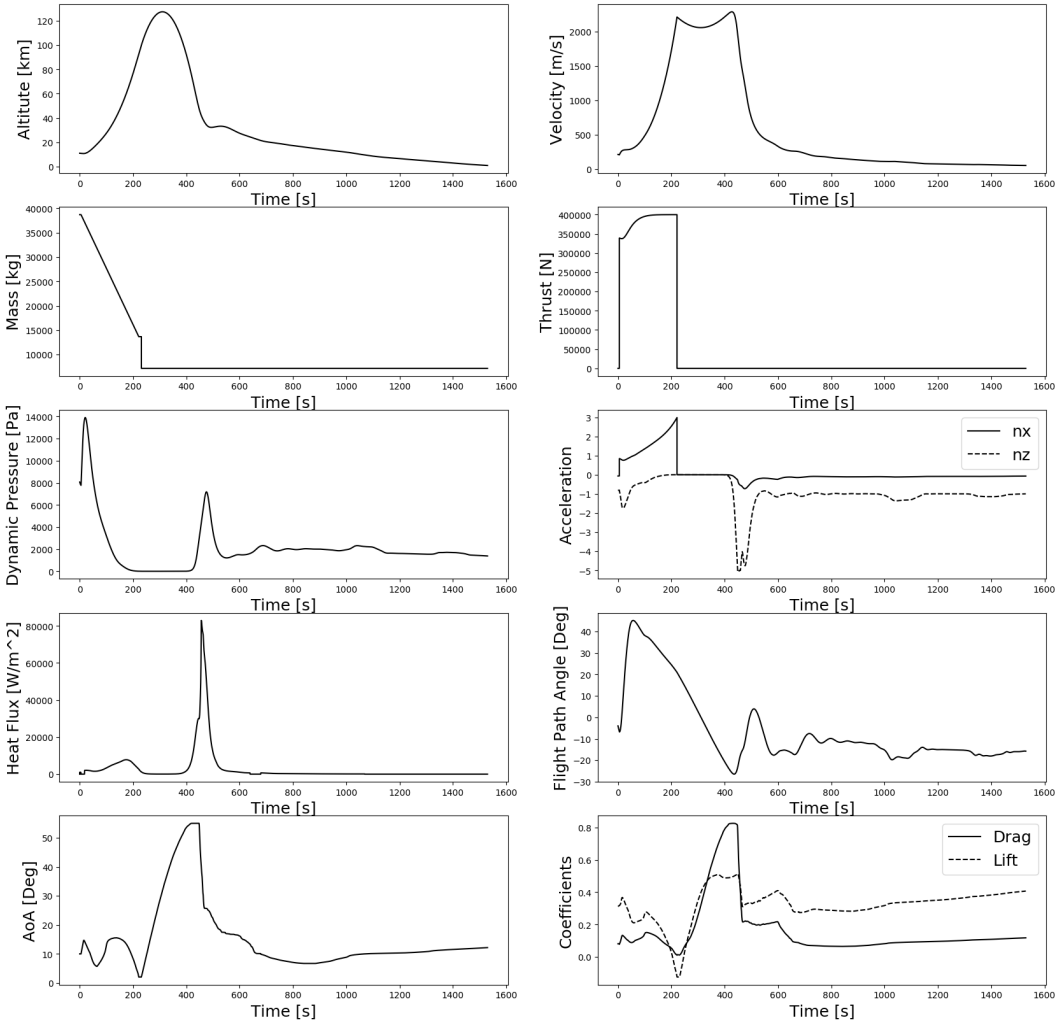


**Figure 11. Converged trajectory**

In order to asses the impact of various constraints, three cases were considered. Starting from a case

with no flight mechanics constraints, trim and stability constraints are gradually added.

### VIII.A. Case 1: Unconstrained

In the first case, no flight mechanics constraints, nor landing constraints, were imposed. As a result, the wings are not needed and the optimizer simply tries to change the spaceplane into a pure rocket by getting rid of the wings. The geometric design variables reach the lower bounds, and the minimum allowed wing area is reached. We observe that with the current mass model, the slope is such that it is better to reduce the mass of the rocket by reducing the size of the wings than to benefit from a lift-assisted climb. Fig. 12 shows the converged path and how the trim and stability conditions are not met. In Fig. 12, the white area represents the allowed flying conditions. The //-hatched area is not allowed by the Aft CoG limit, and the \\-hatched area is not allowed by the Front CoG limit. When these two areas overlap, they form a grid.

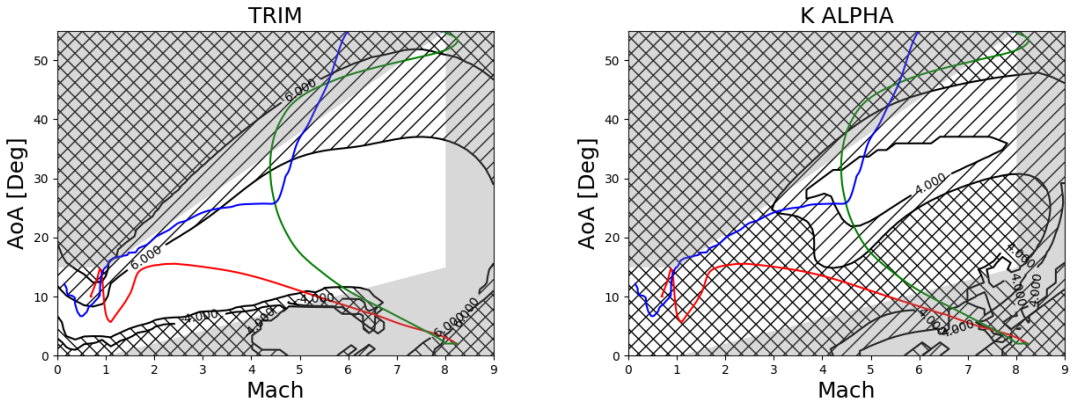


**Figure 12. Case 1: Aft CoG limit (//-hatched area) and Front CoG limit (\\-hatched area)**

It is worth noting that if the mass model is removed, and the optimizer is allowed to increase the wing area without any increase in mass, the converged solution correspond to the maximum allowed wing area. This is to take advantage of a lift-assisted climb which allows to reach a low density atmosphere faster, where the drag is lower.

### VIII.B. Case 2: Trim Constraint

In the second case, a trim constraint expressed in Eq. (20) is imposed. As it turns out, a minimum wing area is reached again. The optimizer prefers to change the trajectory to a slightly less favorable path in order to respect the flight mechanics constraints, than to increase the mass of the spaceplane by modifying its shape.

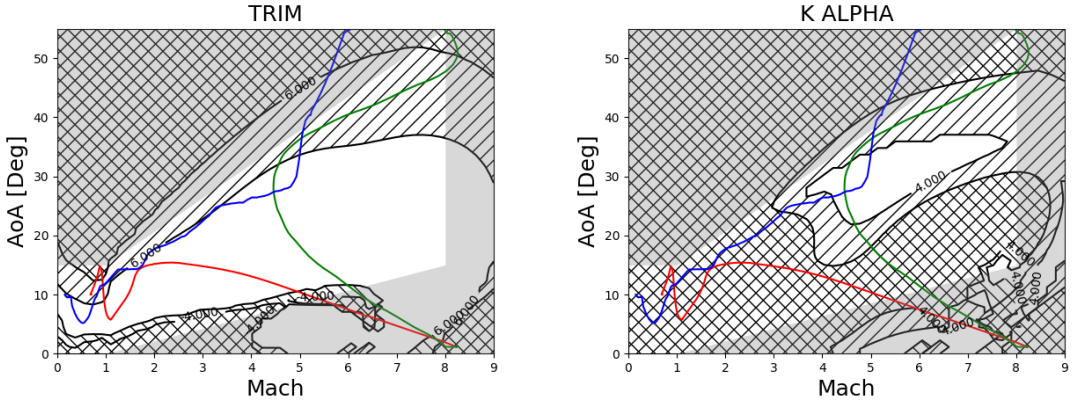


**Figure 13. Case 2: Aft CoG limit (//-hatched area) and Front CoG limit (\\-hatched area)**

In Fig. 13, the red path corresponds to the powered ascent phase where trim is achieved by Thrust Vectoring Control (TVC). The green path corresponds to the unpowered gliding trajectory at altitude for which the aerodynamic control surfaces are unusable and trim is achieved using a Reaction Control System (RCS). Finally, the blue path, where aerodynamic effects are sufficient to help control the spaceplane, is the only path where trim constraint of Eq. (20) should be met.

### VIII.C. Case 3: Trim and Static Stabilization Constraints

In the third case, a trim constraint, Eq. (20), and a stabilization constraint, Eq. (16), are imposed. The wing planform, the size of the elevons, and the location of their hinge line must be modified so as to increase the effect of the elevon deflection and to satisfy the stabilization constraint.

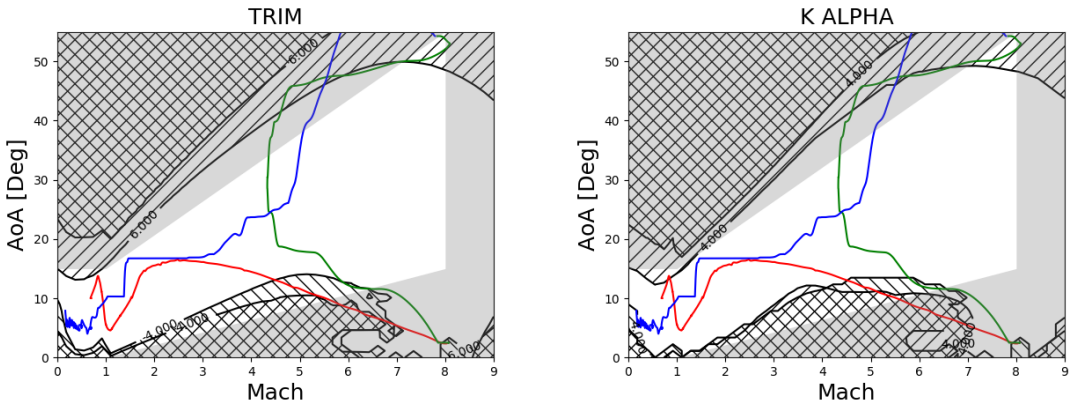


**Figure 14. Case 3: Aft CoG limit (//-hatched area) and Front CoG limit (\\-hatched area)**

In comparison to Cases 1 and 2, the maximum speed $v_{\mathrm{MECO}}$ decreased substantially: 2167.65 m/s as opposed to 2210.75 m/s in Case 1. The wing planform modification is shown in Fig. 15. This shows how important it is to take rigid body characteristics, such as trim and stability, into consideration even at the conceptual design level.

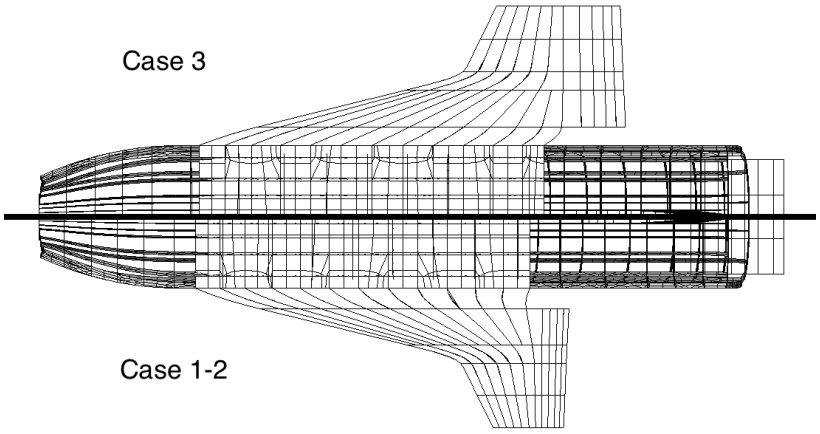


**Figure 15. Wing planform comparison**

## IX. Conclusion

Using an NLP-based All-At-Once MDO architecture, the conceptual design of a spaceplane was performed by simultaneously optimizing its flight trajectory and its configuration.

A parametric geometry for the spaceplane was generated using GeoMACH. The optimal control problem was implemented using GPOPS-II and the optimization was carried out using SNOPT. Aerodynamic coeffi-

cients were calculated using SU2. Weight estimation was based on structural optimization using the Toolkit for the Analysis of Composite Structures (TACS) and empirical methods from the Hypersonic Aerospace Sizing Analysis (HASA) method. For the structure, the common approach of lumping the restrictions on admissible stresses into a Kreisselmeier-Steinhauser (KS) function was used. Kriging models were created using Surfpack to give aerodynamic coefficients and mass estimate.

Three cases were successfully optimized. The first case, with no flight mechanics constraints, serves as a baseline to measure the impact of adding trim and stability requirements. In the second case, a trim constraint was enforced. Results showed that instead of modifying the spaceplane's configuration, the optimizer chose to alter the trajectory path. Finally, in the third case, when stabilization is required, the optimizer had no other choice than to modify the planform of the wing and increase the mass of the spaceplane as a result. This resulted in a substantial loss of speed at main engine cut-off, which demonstrates the importance of covering rigid body characteristics, like trim and stability, even at conceptual design level.



## Acknowledgment

The authors would like to acknowledge Rafael Molina, Robin Dufour, Petr Kuchynka and Jeremie Despraz for their insights.

## References

[1]N. Yokoyama, S. Suzuki, T. T. H. T. T. K., "Multidisciplinary design optimization of a space plane considering rigid body characteristics," *Journal of Spacecraft and Rockets*, Vol. 44.1, 2007, pp. 121–131.

[2]Tsuchiya, Takeshi, Y. T. and Taguchi, H., "Multidisciplinary design optimization for hypersonic experimental vehicle," *AIAA journal*, Vol. 45.7, 2007, pp. 1655–1662.

[3]Tsuchiya, T. and Mori, T., "Optimal conceptual design of two-stage reusable rocket vehicles including trajectory optimization," *Journal of Spacecraft and Rockets*, Vol. 41.5, 2004, pp. 770–778.

[4]Robin Dufour, J. d. M. and Elham, A., "Trajectory driven multidisciplinary design optimization of a sub-orbital spaceplane using non-stationary Gaussian process," *Springer, Struct Multidisc Optim*, Vol. 52, 2015, pp. 755–771.

[5]Hwang, J. T. and Martins, J. R. R. A., "GeoMACH: Geometry-Centric MDAO of Aircraft Configurations with High Fidelity," *American Institute of Aeronautics and Astronautics*.

[6]John T. Hwang, G. K. W. K. and Martins, J. R. R. A., "Geometry and Structural Modeling for High-Fidelity Aircraft Conceptual Design Optimization," *15th AIAA/ISSMO Multidisciplinary Analysis and Optimization Conference*, 2014.

[7]Martins, J. R. R. A. and Hwang, J. T., "Review and Unification of Methods for Computing Derivatives of Multidisciplinary Computational Models," *AIAA Journal*, Vol. 51, No. 11, November 2013, pp. 2582–2599.

[8]Nguyen X. Vinh, Adolf Busemann, R. D. C., "Hypersonic and Planetary Entry Flight Mechanics," *Ann Arbor, Mich., University of Michigan Press*, 1980.

[9]Gill, P., M. W. and Saunders, M., "SNOPT: An SQP Algorithm for Large-Scale Constrainted Optimization," *Society for Industrial and Applied Mathematics*, Vol. 47, No. 1, February 2005, pp. 99–131.

[10]Patterson, M. A. and Rao, A. V., "GPOPS-II: A MATLAB Software for Solving Multiple-Phase Optimal Control Problems Using hp-Adaptive Collocation Methods and Sparse Nonlinear Programming," *University of Florida*.

[11]Garg, D., P. M. H. W. W. R. A. V. B. D. A. and Huntington, G. T., "A unified frame- work for the numerical solution of optimal control problems using pseudospectral methods," *Automatica*, Vol. 46, No. 11, 2010, pp. 1843–1851.

[12]Garg, D., H. W. W. and Rao, A. V., "Pseudospectral methods for solving infinite-horizon optimal control problems," *Automatica*, Vol. 47, No. 4, 2011, pp. 829–837.

[13]Garg, D., P. M. F. C. D. C. H. G. H. W. W. and Rao, A. V., "Direct trajectory optimization and costate estimation of finite-horizon and infinite-horizon optimal control problems using a Radau pseudospectral method," *Computat. Optim. Appl.*, Vol. 49, No. 2, 2011, pp. 335–358.

[14]Patterson, M. A. and Rao, A. V., "Exploiting sparsity in direct collocation pseudospectral methods for solving optimal control problems." *Journal Spacecraft Rockets*, Vol. 49, No. 2, 2012, pp. 364–377.

[15]F. Palacios, M. R. Colonno, A. C. A. A. C. S. R. C. T. D. E. A. K. L. T. W. L. T. W. R. T. and Alonso, J. J., "Stanford University Unstructured (SU2): An open-source integrated computational environment for multi-physics simulation and design," *AIAA Paper, 51st AIAA Aerospace Sciences Meeting and Exhibit*, Vol. 2013-0287, 2013.

[16]P.L. George, F. Hecht, E. S., "Fully automatic mesh generator for 3d domains of any shape," *Impact of Comp. in Sci. and Eng.*, Vol. 2, 1990, pp. 187–218.

[17]Loseille, A. and Lohner, R., "Cavity-based operators for mesh adaptation," *51st AIAA Aerospace Sciences Meeting including the New Horizons Forum and Aerospace Exposition, Aerospace Sciences Meetings*, Jan 2013.

[18]Frederic Alauzet, D. M., "A Closed Advancing-Layer Method with Changing Topology Mesh Movement for Viscous Mesh Generation," *Proceedings of the 22nd International Meshing Roundtable*, 2013, pp. 241–261.

[19]J. R. Martins, N. M. P., "On Structural Optimization Using Constraint Aggregation," *6th World Congress on Structural and Multidisciplinary Optimization*, 2005.

[20]Kreisselmeier, G. and Steinhauser, R., "Systematic control design by optimizing a vector performance index," *International Federation of Active Controls Syposium on Computer-Aided Design of Control Systems, Zurich, Switzerland*, 1979.

[21]Andrew B. Lambe, Graeme J. Kennedy, J. R. R. A. M., "Multidisciplinary Design Optimization of an Aircraft Wing via a Matrix-Free Approach," *15th AIAA/ISSMO Multidisciplinary Analysis and Optimization Conference*, 2014.

[22]Harloff, G. J. and Berkowitz, B. M., "HASA: Hypersonic Aerospace Sizing Analysis for the Preliminary Design of Aerospace Vehicles," *NASA CR-182226*, 1988.

[23]Frey, P., "mshint," *Pierre and Marie Curie University; https://www.ljll.math.upmc.fr/frey/ftp/archives/mshint.2010.05.07.tgz*.

[24]Frederic Alauzet, M. M., "P1-Conservative solution interpolation on unstructured triangular meshes," *Numerical Methods in Engineering*, 2010.

[25]Kennedy, G. J. and Martins, J. R. R. A., "A parallel finite-element framework for large-scale gradient-based design optimization of high-performance structures," *Finite Elements in Analysis and Design*, Vol. 87, Sept. 2014, pp. 56–73.

[26]Koehler, J. R. and Owen, A. B., "Computer experiments," *Handbook of Statistics*, Vol. 13, 1996, pp. 261–308.

[27]Giunta, A. A. and Watson, L. T., "A comparison of approximation modeling techniques: polynomial versus interpolating models," *AIAA 98-4758 in Proceedings of the 7th AIAA/USAF/NASA/ISSMO Symposium on Multidisciplinary Analysis and Optimization*, 1998, pp. 392–404.

[28]Simpson, T. W., M. T. M. K. J. J. and Mistree, F., "Kriging Metamodels for Global Approximation in Simulation- Based Multidisciplinary Design Optimization," *AIAA Journal*, Vol. 39, No. 12, 2001, pp. 2233–2241.

[29]Romero, V. J., S. L. P. and Giunta, A. A., "Construction of response surfaces based on progressive-lattice- sampling experimental designs," *Structural Safety*, Vol. 26, No. 2, 2004, pp. 201–219.

[30]Masato Sekishiro, G. V. and Balabanov, V., "Combined Kriging and Gradient-Based Optimization Method," *11th AIAA/ISSMO Multidisciplinary Analysis and Optimization Conference*.

[31]Shawn E. Gano, H. K. and Brown, D. E., "Comparison of Three Surrogate Modeling Techniques: Datascaper, Kriging, and Second Order Regression," 2006.

[32]Anthony A. Giunta, Laura P. Swiler, S. L. B. and Eldred, M. S., "The Surfpack Software Library for Surrogate Modeling of Sparse Irregularly Spaced Multidimensional Data," .

[33]Sacks, J., W. W. J. M. T. J. and Wynn, H. P., "Design and Analysis of Computer Experiments," *Statistical Science*, Vol. 4, No. 4, 1989, pp. 409–423.

[34]Giunta, A. A. and Watson, L. T., "A Comparison of Approximation Modeling Techniques: Polynomial Versus Interpolating Models," *AIAA-98-4758*, 1998.

[35]Simpson, T.W., M. T. K. J. and Mistree, F., "Kriging Models for Global Approximation in Simulation-Based Multidisciplinary Design Optimization," *AIAA Journal*, Vol. 39, No. 12, 2001, pp. 2233–2241.

[36]McKay, M. D., B. R. J. and Conover, W. J., "A Comparison of Three Methods for Selecting Values of Input Variables in the Analysis of Output from a Computer Code," *Technometrics*, Vol. 21, 1979, pp. 239–245.

[37]Jansen, P. and Perez, R., "Constrained structural design optimization via a parallel augmented Lagrangian particle swarm optimization approach," *Computers and Structures*, Vol. 89, No. 1314, 2011.

[38]Perez, R., J. P. and Martins, J., "pyOpt: A Python-Based Object-Oriented Framework for Nonlinear Constrained Optimization," *Structures and Multidisciplinary Optimization*, Vol. 45, No. 1, January 2012, pp. 101–118.

[39]Greer, H. D., "Summary of Directional Divergence Characteristics of Several High-Performance Aircraft Configurations," *NASA Technical Note*, Vol. D-6993, 1972.

[40]Roskam, D. J., "Airplane Design, Part VII: Determination of Stability, Control and Performance Characteristics: FAR and Military Requirements," .

[41]Caughey, D. A., "Introduction to Aircraft Stability and Control," *Course Notes for M&AE 5070 Cornell University*.

[42]Anon., "Flying Qualities of Piloted Airplanes," *MIL SPEC, MIL-F-8785C, U.S. Government Printing Office, Washington, DC*, Nov 1980.

[43]Charles A. Mader, J. R. R. A. M., "Computing Stability Derivatives and Their Gradients for Aerodynamic Shape Optimization," *AIAA Journal*, Vol. 52, No. 11, November 2014.

[44]Nitin D. Bhagat, E. J. A. and Allison, D., "Geometry Driven High Fidelity Stability Derivatives Using An Automated CFD Analysis Process," *16th AIAA/ISSMO Multidisciplinary Analysis and Optimization Conference*, 2015.

[45]Balling, R. J. and Wilkinson, C. A., "Execution of Multidisciplinary Design Optimization Approaches on Common Test Problems," *AIAA Journal*, Vol. 35, No. 1, 1997, pp. 178–186.